Small-scale robots inspired by aquatic interfacial biolocomotion

Dongjin Kim, Chan Jin Park, Je-Sung Koh,* and Jonghyun Ha*

Bioinspired semiaquatic robots have a remarkable ability to effectively navigate on the water surface. In this article, we explore the design of these biomimetic robotic systems and their body scale-dependent governing forces behind the motion. First, the role of surface tension in enabling hydrophobic objects to remain afloat despite having greater density than water and the effect of morphology, especially the presence of hair-like structures, on the flotation stability are discussed. Then the forces that drive the diverse motions of natural organisms and robots on the air/water interface are investigated. We highlight that while small organisms and robots generate motion utilizing surface tension-based force, large ones primarily exploit inertial drag for propulsion. We show the correlation between the performance and body size in both small and large natural organisms, and how they adjust the shape and speed of legs to optimize the propulsion. To optimize these distinct propulsion forces, the shape and speed of the driving legs are adjusted, thereby maximizing momentum while maintaining high efficiency. This article aims to provide insights on the design and operating mechanism of semiaquatic robots and to bridge the gap between the study of biological locomotion and its mechanical analogs.

Introduction

Survival techniques in nature occasionally inspire us and provide novel solutions to the engineering issues that we encounter as they are the result of extensive optimization sculpted by evolution. One example is the water harvesting of a desert beetle.[1] Despite inhabiting arid and desolate environments, it has been discovered that this beetle proficiently gathers water from the atmosphere leveraging its microtextured surfaces. This fundamental biomimetic study paved the way to the development of various functional surfaces for water-harvesting systems.[2] In addition to beetles' survival, water striders exhibit swift yet graceful locomotion when encountered with a predator.[3] Intriguingly, water striders demonstrate remarkable stability when floating on water and even when executing dynamic movements to evade predators. Such interfacial biolocomotion resulted in the development of various-sized robots that can execute diverse motions such as jumping, rowing, and galloping on water.[4–7] **Figure 1** shows various organisms and robots with diverse body sizes that can move on water. Depending on their body sizes, distinct locomotion mechanisms are employed, such that for large organisms

and robots, inertia-dominant drag mainly governs the motion whereas motions of small organisms and robots are governed by surface tension-dominant drag.[8,9]

The design of semiaquatic robots that can move on the water surface is often inspired by these organisms. This is because organisms have evolved to maximize their efficiency when moving on water, and the morphological shape of the body and legs are suitably developed to generate a dominant hydrodynamic force. In a small scale, surface tension is much bigger than other forces and similar to the small insects shown in Figure 1, the robots have long and thin legs to maximize surface tension. In a larger scale, inertial drag is the dominant hydrodynamic force, so the robots are equipped with large pads at the ends of legs such as the webfoot or flipper of animals and some robots have large air balls to obtain buoyancy for floating. In this article, the body scale, which determines the dominant force of locomotion, is a comprehensive parameter quantified by two nondimensional numbers: Weber number (We) and Bond number (Bo) to include the body size and speed.
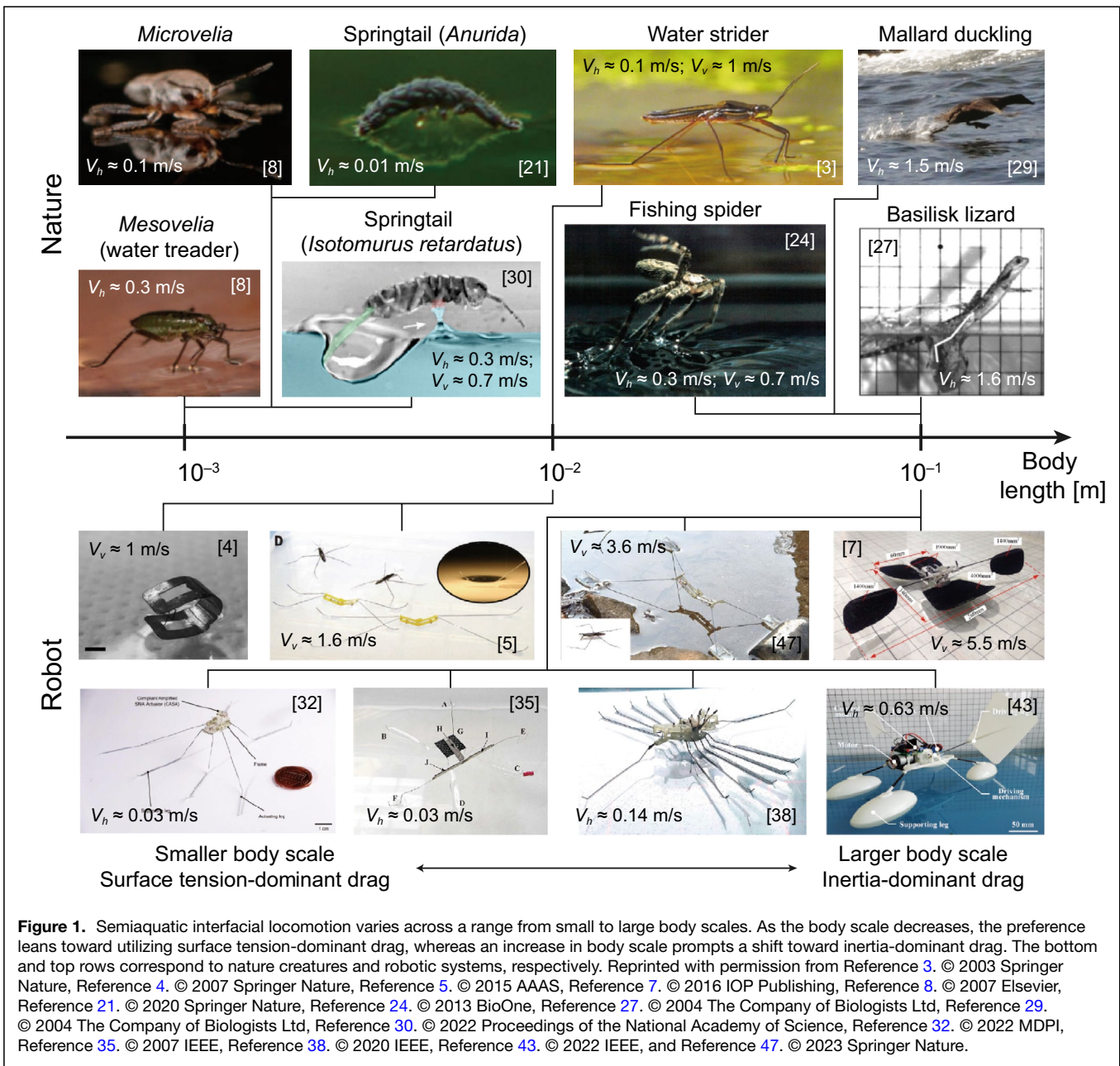
In the following, the physics of floating and the mechanism of the interfacial biolocomotion are first discussed. Then, we

Dongjin Kim, Department of Mechanical Engineering, Ajou University, Suwon, Republic of Korea; rlaehdwlswt@ajou.ac.kr
Chan Jin Park, Department of Chemical and Biological Engineering, Princeton University, Princeton, USA; cp4553@princeton.edu
Je-Sung Koh, Department of Mechanical Engineering, Ajou University, Suwon, Republic of Korea; jskoh@ajou.ac.kr
Jonghyun Ha, Department of Mechanical Engineering, Ajou University, Suwon, Republic of Korea; hajh@ajou.ac.kr
*Corresponding author
Dongjin Kim and Chan Jin Park have contributed equally to this work.

Figure 1. Semiaquatic interfacial locomotion varies across a range from small to large body scales. As the body scale decreases, the preference leans toward utilizing surface tension-dominant drag, whereas an increase in body scale prompts a shift toward inertia-dominant drag. The bottom and top rows correspond to nature creatures and robotic systems, respectively. Reprinted with permission from Reference 3. © 2003 Springer Nature, Reference 4. © 2007 Springer Nature, Reference 5. © 2015 AAAS, Reference 7. © 2016 IOP Publishing, Reference 8. © 2007 Elsevier, Reference 21. © 2020 Springer Nature, Reference 24. © 2013 BioOne, Reference 27. © 2004 The Company of Biologists Ltd, Reference 29. © 2004 The Company of Biologists Ltd, Reference 30. © 2022 Proceedings of the National Academy of Science, Reference 32. © 2022 MDPI, Reference 35. © 2007 IEEE, Reference 38. © 2020 IEEE, Reference 43. © 2022 IEEE, and Reference 47. © 2023 Springer Nature.
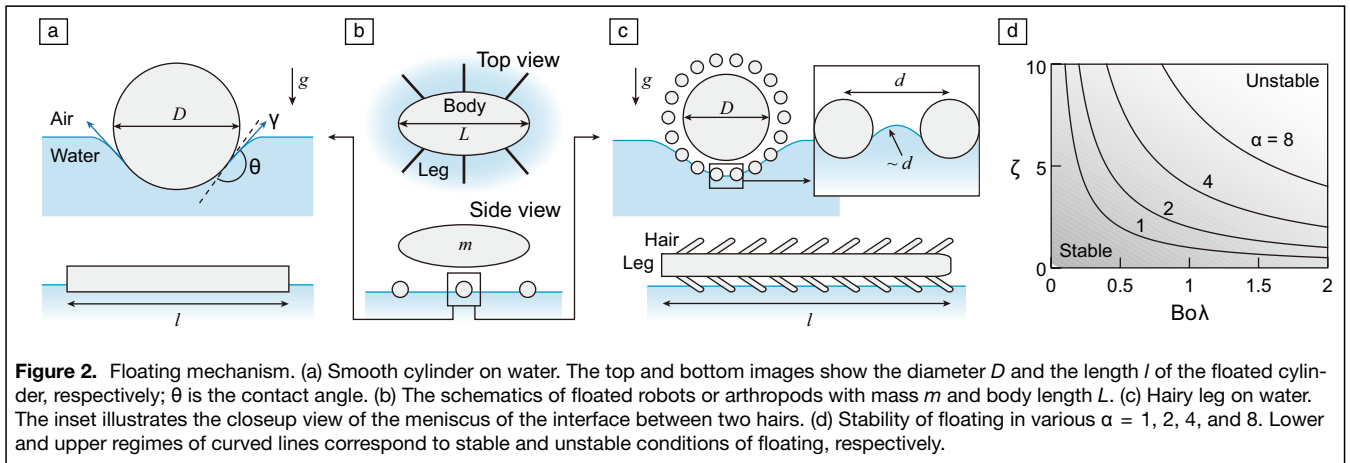
review how biomimetic robots with various sizes adopt distinct mechanisms to move and float on the water. Finally, we plot a universal regime map for the locomotion of both organisms and robots and compare the interfacial locomotion of natural and artificial systems.

Statics: Physics of floating

In this section, we introduce the physics behind the floating slender, hydrophobic objects that have a density larger than that of water.[10–12] This phenomenon is facilitated by the exploitation of surface tension, which acts at the air–liquid–solid interface. We start by considering the simplest geometry of a smooth slender cylinder as shown in **Figure 2**a. Typically, given the extremely small submerged volume of the object, the effect of buoyancy

is generally assumed to be insignificant.[10] Then, the contact angle between air–liquid interfaces, θ, plays an important role in surface tension-dominant floating, where for a hydrophobic surface, the contact angle is obtuse ($\theta > \pi/2$). The stability of the floating state can be analyzed through a force balance between the gravitational force acting on the body, $W \sim mg$, and the surface tension-driven forces at the air–liquid–solid contact line, $F_s \sim \gamma l \sin(\theta - \pi/2)$, where m, g, γ, and l are mass of the object, gravitational acceleration, surface tension, and the wetted length, respectively. For a superhydrophobic surface where $\theta \approx \pi$, the expression can be reduced to $F_s \sim \gamma l$. Thus, an object can stably remain afloat on the water surface when this surface tension-driven force exceeds its own weight ($F_s > W$), as shown in Figure 2b. By establishing an equilibrium between

Figure 2. Floating mechanism. (a) Smooth cylinder on water. The top and bottom images show the diameter D and the length l of the floated cylinder, respectively; θ is the contact angle. (b) The schematics of floated robots or arthropods with mass m and body length L. (c) Hairy leg on water. The inset illustrates the closeup view of the meniscus of the interface between two hairs. (d) Stability of floating in various $\alpha = 1, 2, 4,$ and 8. Lower and upper regimes of curved lines correspond to stable and unstable conditions of floating, respectively.

two characteristic forces $W \sim F_s$, and subsequently normalizing the equation with the liquid density, ρ_l, we obtain $\zeta \sim (Bo\lambda)^{-1}$, where $\zeta = \rho_s/\rho_l$, $Bo = (\rho_l L^2 g)/\gamma$, and $\lambda = L/l$ are the density ratio, the Bond number, and the wetting portion. This relationship provides the design parameters for semiaquatic robots with slender legs to achieve stable flotation on water.

The flotation stability can be significantly enhanced by introducing the hair-like surface morphology.[8,13,14] For hydrophobic surfaces, this surface roughness results in water-repelling behavior by trapping the air within the complex surface structures, a phenomenon known as the Cassie state.[15,16] In the hairy configuration, the capillary pressure arises at the small gap between the hairs to repel the water, as shown in Figure 2c. Considering the capillary pressure $\Delta p \sim \gamma/d$ and the effective wetted area $A \sim Dl$, we get the water-repellent force $F_c \sim \gamma l D/d$. Substituting F_c for F_s in the force balance equation ($W \sim F_s$), we obtain
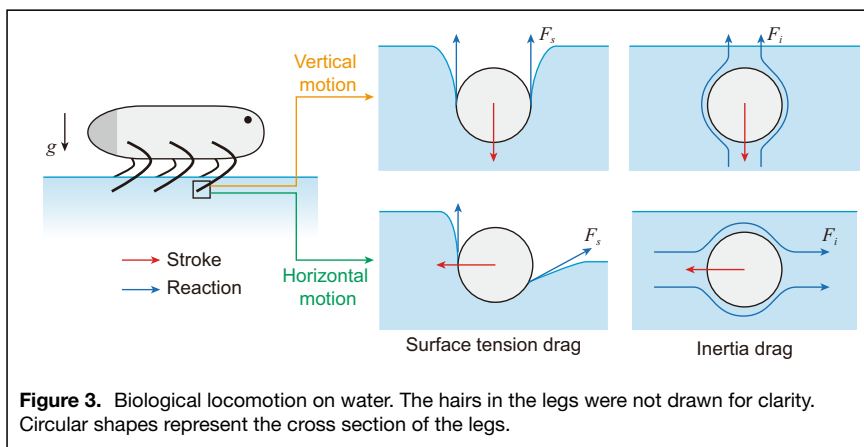
$$\zeta \sim \alpha(Bo\lambda)^{-1}, \qquad 1$$

where $\alpha = D/d$. This equation explains the mechanism by which robots or organisms heavier than water can achieve stable flotation using their hairy legs. Figure 2d shows the stable and unstable regime of flotation for various α. As can be noted, the increase of α results in an increased stable region beneath the curve. This suggests that hairy surfaces enable materials with a higher density to stably float on the water surface. The typical value of alpha in the legs of aquatic insects is known to be on the order of 10, which significantly enhances the floating ability.

Kinetics: Interfacial locomotion mechanism

We now discuss how the organisms achieve dynamic motions while maintaining afloat on the water surface. Semiaquatic organisms propel themselves on water by exerting force on the liquid, which in turn generates reactive forces. As shown in **Figure 3**, the direction of locomotion—either vertical or horizontal—is determined by the direction of the stroke, where the orange and green lines, respectively, show vertical and horizontal locomotion. Based on the length of the body, the dominant reaction forces of the reaction can be either the inertia-dominated drag of large organisms or the surface tension-dominated drag of smaller ones (see Figure 1). On the other hand, certain organisms (*Microvelia* and *Dianous coerulescens*) have a unique method of locomotion on water surfaces.[17,18] Instead of producing mechanical motion, they secrete chemical substances from the posterior edge of the body, instigating Marangoni effects that enable movements.

We consider the case when the organisms apply force on the fluid via dynamic leg motion. When the leg exerts force on the liquid, a reaction drag is induced, which consists of several forces: $F \sim F_i + F_s + F_b$, where F_s corresponds to the surface tension-driven force ($F_s \sim \gamma L$) and F_b represents buoyancy ($F_b \sim \rho_l L^3 g$). The inertial force F_i is governed by dynamic pressure, $F_i \sim \rho_l U^2 L^2$, where U is velocity. Upon considering these three forces (F_i, F_s, and F_b), we can derive two dimensionless group numbers.[9,19] The ratio of F_i to F_s yields the Weber number, We = $\rho_l U^2 L/\gamma$, and the ratio of F_b to F_s provides the Bond number, Bo = $\rho_l L^2 g/\gamma$, which offers useful insights when identifying the dominant reaction drag accompanied with the motion.

Figure 3. Biological locomotion on water. The hairs in the legs were not drawn for clarity. Circular shapes represent the cross section of the legs.

When both L and U are small, capillary force dominates over the inertial and hydrostatic forces and the organism propels mainly exploiting the capillary force. As illustrated in Figure 3, when locomotion is driven by capillary forces, the movement of the leg distorts the air–water interface rather than breaking it.[20,21] The water striders, which are capable of exhibiting both horizontal and vertical motion on the water surface, serve as a representative example.[3,5] In addition to simply using the capillary force, it has been recently revealed that the water striders tune the leg stroke speed to achieve maximum jumping speed without breaking the interface.[22,23]

Given that the magnitude of F_s is directly proportional to the characteristic length ($F_s \sim \gamma L$), it can be challenging for organisms with larger body sizes (proportional to L^3) to generate sufficient force relying solely on capillary force. Therefore, it is common for larger organisms to propel using inertial force rather than capillary force. For instance, it is known that inertial and hydrostatic forces govern the galloping of fishing spiders,[24] "running" of basilisk lizards,[25–27] and hydroplaning of ducklings on water,[28,29] whose body lengths all exceed 0.1 m. Interestingly, there are also small organisms that can move their legs so fast that inertial force is the dominant force. For instance, although springtails (*Isotomurus retardatus*) are usually smaller in size compared to typical water striders, they exhibit fast leg stroke that their vertical and horizontal motions are both governed by the inertial force (see Figure 1).[30] Remarkably, it has been recently reported that in contrast to small water striders that exploit capillary force, large water striders use inertial drag to evade the attacks from underwater predators.[31]

Exploration of biomimetic arthropod-inspired robotics

Semiaquatic robots are designed by considering the scale of the system and utilize the primary driving force derived from the water surface as shown in **Figure 4**. On the water surface, the momentum of the robot can be generated by the reaction force exerted on 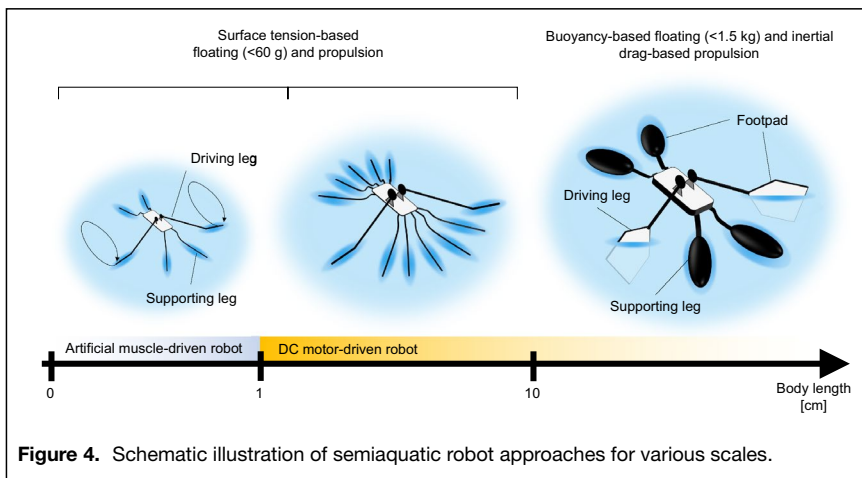its legs, which are the surface tension or the inertial drag from the water. To take advantage of a different propulsion force, the shape and speed of the driving legs are adjusted to optimize movement speed while maintaining high efficiency.

In the following section, various robots moving on the water surface are presented, and that show how the hydrodynamics of organisms are considered in the morphological design of the robot. As shown in Figure 4, we can find typical designs of the robots depending on the scale. In a small scale, the robot has the minimum number of thin and light legs to generate a surface tension force high enough for floating and walking on the water. The robot in this scale also utilizes an artificial muscle actuator for the light weight. As the system gets bigger, the number of legs increases, and the shape of the legs is designed to make longer contact lengths with the water surface. When the system exceeds the surface tension-dominant scale, the buoyancy and the inertial drag are the dominant forces for floating and propulsion. Therefore, the bigger robots generally have airballs for the buoyancy and large pads for the inertial drag as shown in Figure 4.
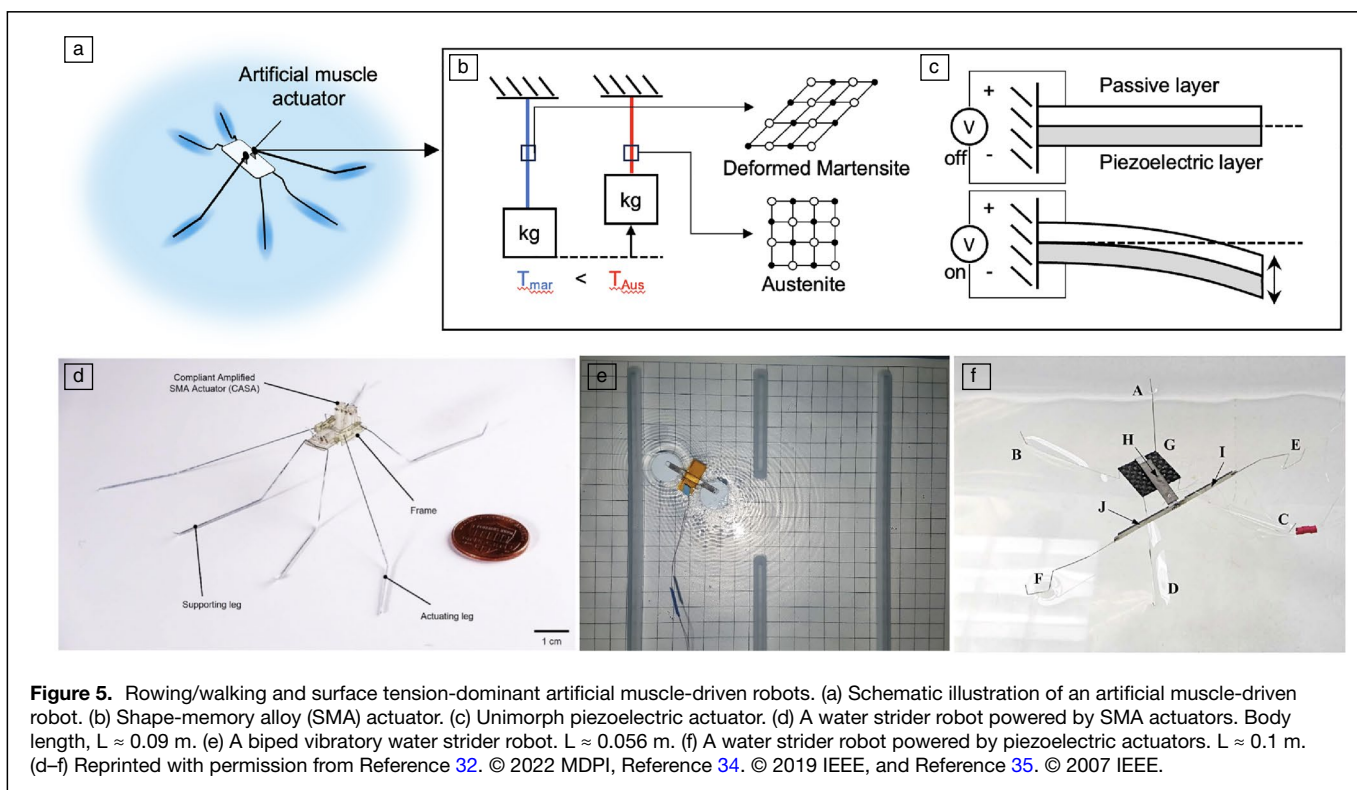
Horizontal locomotion in robots

Rowing/walking locomotion is typically obtained by the rowing motion of the actuation legs while the other supporting legs support the robot on the water surface as shown in **Figure 5**a. Surface tension-dominant robots are generally lighter than drag-dominant robots. To reduce the total weight of the robots, rowing/walking robots employ artificial muscle actuators such as a shape memory alloy (Figure 5b) and a piezoelectric actuator (Figure 5c). The lightest water-walking robot (0.22 g) capable of multiple rowing motions uses a shape-memory alloy (SMA) actuator shown in Figure 5d.[32] The most prevalent SMA used to actuate a microrobot is nickel-titanium (NiTi), which shows remarkably high-power density (~50 kW/kg).[33] However, SMAs have a low strain, and it has been shown that this can be overcome by amplifying the strain of SMA using compliant beams made of glass-reinforced epoxy laminate as shown in Figure 5d.

Both the water strider robots in Figure 5e and f are actuated by piezoelectric actuators for the light weight.[34,35] Lead zirconate titanate (PZT) is the most common material used for piezoelectric actuators. The piezoelectric actuators have a low strain, even lower than the SMA. The milli-scale biped robot in Figure 5e has two circular feet. Utilizing vibratory excitation, the feet apply thrust to the water supported by the surface tension. The water robot in Figure 5f has a different operation mechanism with the same material as the actuator. A T-shape structure composed of three piezoelectric unimorph actuators produces the elliptical sculling motion of the driving legs.

Surface tension-based floating (<60 g) and propulsion

Buoyancy-based floating (<1.5 kg) and inertial drag-based propulsion

Footpad

Driving leg

Driving leg

Supporting leg

Supporting leg

Artificial muscle-driven robot

DC motor-driven robot

Body length [cm]

0   1   10

Figure 4. Schematic illustration of semiaquatic robot approaches for various scales.

Figure 5. Rowing/walking and surface tension-dominant artificial muscle-driven robots. (a) Schematic illustration of an artificial muscle-driven robot. (b) Shape-memory alloy (SMA) actuator. (c) Unimorph piezoelectric actuator. (d) A water strider robot powered by SMA actuators. Body length, L ≈ 0.09 m. (e) A biped vibratory water strider robot. L ≈ 0.056 m. (f) A water strider robot powered by piezoelectric actuators. L ≈ 0.1 m. (d–f) Reprinted with permission from Reference 32. © 2022 MDPI, Reference 34. © 2019 IEEE, and Reference 35. © 2007 IEEE.

The water strider robots illustrated in **Figure 6**a are actuated by DC motors. In the case of surface tension-dominant robot actuated by DC motors, these robots weigh between 3 and 22 g. To support a comparatively heavy body weight, their legs are coated with a hydrophobic material or structure (Figure 6b–c) and they have at least 10 supporting legs or circular footpads (Figure 6d). The aquatic microrobot in Figure 6e has supporting legs that are superhydrophobic copper wires covered with nanoribbons ($Cu(OH)_2$) causing the plastron effect.[36] The water strider robot in Figure 6f employs a cam-link mechanism to generate an ellipse-like spatial trajectory similar to that of a water strider. The robot is also designed to move at the maximum speed by increasing the duty cycle of the motor just before breaking the water surface.[37] The other version of this robot has flexible driving legs that allow for an effective increase of the critical rowing speed without the legs penetrating the water surface.[38]

The water strider robots shown in Figure 6g–i are untethered, free from an electric external wire for the control and power supply.[6,39,40] The tension of even a thin electric wire causes the robot to move or to be dragged in the undesired direction, due to the robot's light weight and low shear force between the robot and the water surface. As the water strider in nature has hairy legs for water-repellent characteristics, various kinds of microfabricated hydrophobic legs are introduced in Figure 6g.[39] The water strider robot in Figure 6i uses circular footpads for high payload capability.[6]

Drag-dominant robots typically have driving legs with large pads to increase the drag as shown in **Figure 7**a. To increase the speed of the leg with a large pad, robots have a large DC motor or use spring-based mechanisms to generate high energy output. To support the heavy weight of the robot on the water surface, the robot employs a large hydrophobic pad such as nickel foam (Figure 7b) and a large hollow footpad (Figure 7c) to exploit buoyancy.

The water strider robots shown in Figure 7d–f are a typical design of the drag-dominant robot that has a similar locomotion mechanism as surface tension-dominant robots.[41–44] The water stride robot in Figure 7d utilized superhydrophobic nickel foam sheets for its legs with a spring-based actuating mechanism.[41] Unlike the light robots supported by surface tension, the drag-dominant water strider robots rely on buoyance force with four hollow ellipsoids as supporting legs in Figure 7e.[43] Note that the experimental result shows that the speed of drag-dominant robot increases as the duty cycle of the motor increases. However, the surface tension-dominant robots can only increase speed before the driving legs break the water surface.

Vertical motion of robots

The jumping robots on the water surface have an energy storing and releasing mechanism to generate high power in an instance shown in **Figure 8**. With the exception of the robot in Figure 8d, the jumping robots are designed for a single powerful jump, unlike most of the rowing/walking robots capable of stable repeated multiple motions. The jumping water strider robot in Figure 8a generates high power by a torque-reversal mechanism, which allows the robot to store large energy.[5]
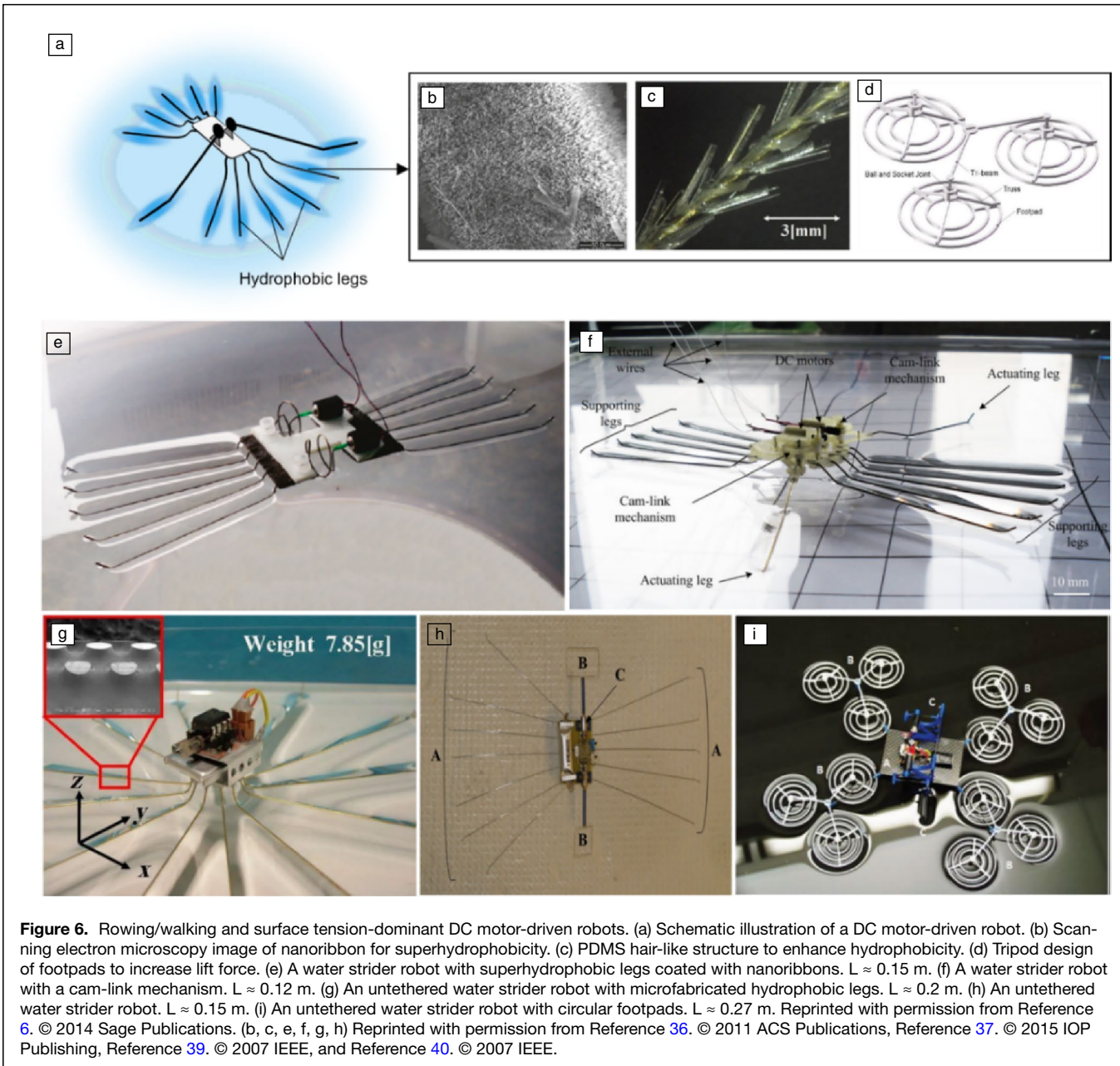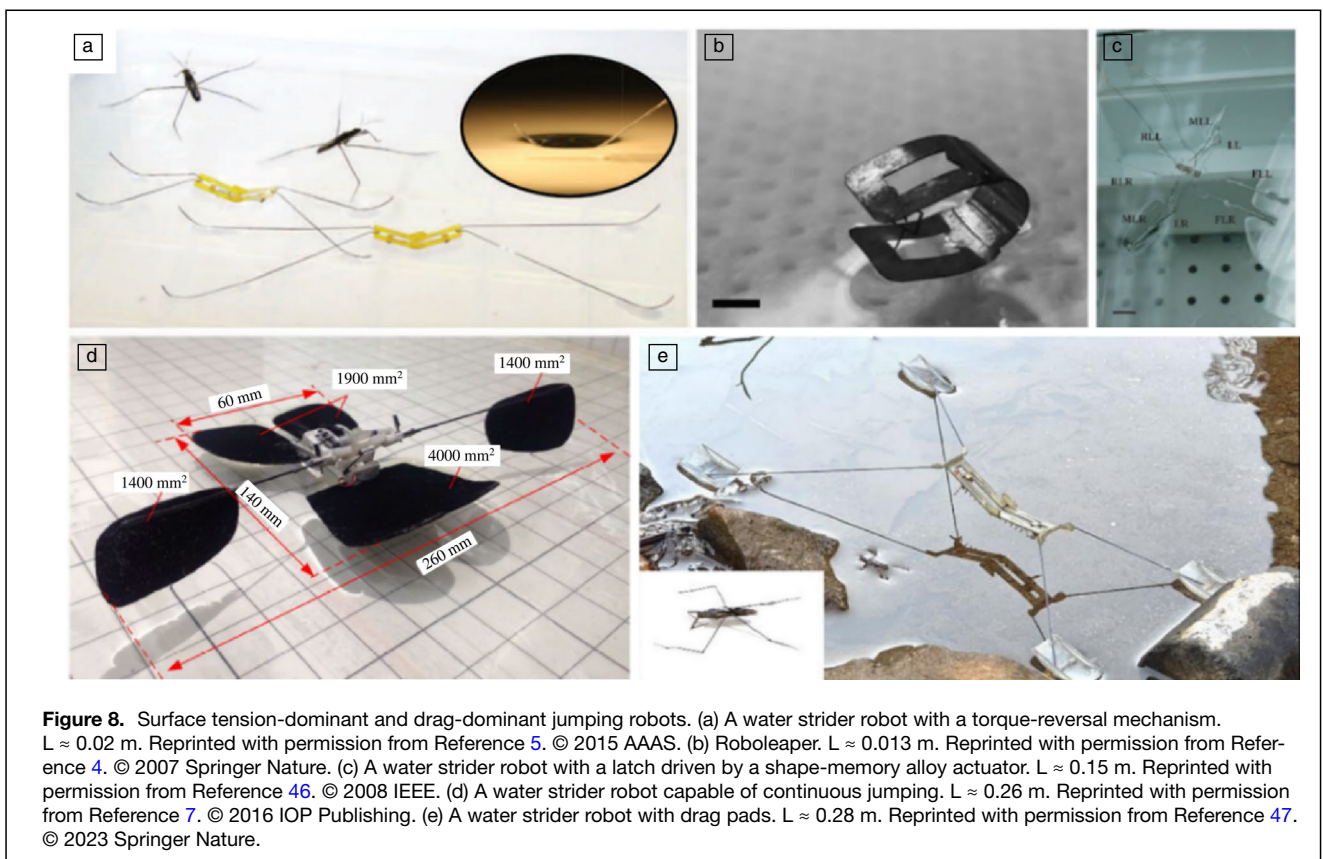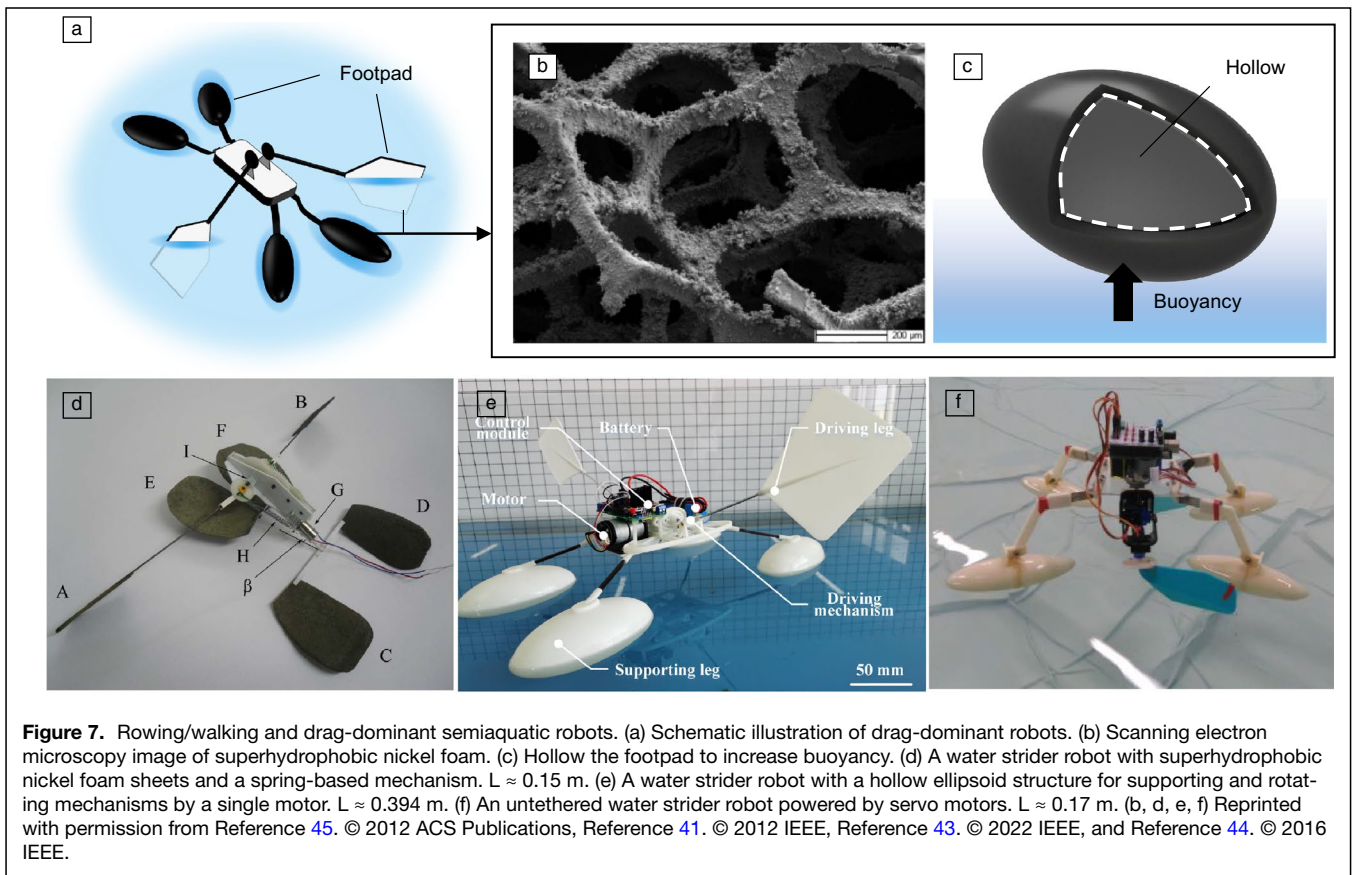
Figure 6. Rowing/walking and surface tension-dominant DC motor-driven robots. (a) Schematic illustration of a DC motor-driven robot. (b) Scanning electron microscopy image of nanoribbon for superhydrophobicity. (c) PDMS hair-like structure to enhance hydrophobicity. (d) Tripod design of footpads to increase lift force. (e) A water strider robot with superhydrophobic legs coated with nanoribbons. L ≈ 0.15 m. (f) A water strider robot with a cam-link mechanism. L ≈ 0.12 m. (g) An untethered water strider robot with microfabricated hydrophobic legs. L ≈ 0.2 m. (h) An untethered water strider robot. L ≈ 0.15 m. (i) An untethered water strider robot with circular footpads. L ≈ 0.27 m. Reprinted with permission from Reference 6. © 2014 Sage Publications. (b, c, e, f, g, h) Reprinted with permission from Reference 36. © 2011 ACS Publications, Reference 37. © 2015 IOP Publishing, Reference 39. © 2007 IEEE, and Reference 40. © 2007 IEEE.

The jumping motion is triggered by SMA by releasing stored energy. The robot is also designed to jump on the water with a maximum takeoff velocity (1.6 m/s) before breaking the water surface. The Roboleaper also stores and releases energy for jumping as shown in Figure 8b.[4] The robot stores energy in the leaf spring and releases it when the latch is removed. The Roboleaper is the smallest water-jumping robot inspired by a springtail reported so far.

The water strider robot in Figure 8c exhibits a relatively low takeoff velocity compared to other jumping robots.[46] The robot designed to utilize surface tension could have broken the water surface and utilized the drag resulting in low velocity. To utilize drag under the water, the robot should have a large area of pads as shown in Figure 8d.[7,45] This water strider robot can jump continuously with large hydrophobic nickel foams. For continuous jumps, the supporting legs are curved at the tip for stable landing. A smaller robot with such pads for drag-based reaction force is shown in Figure 8e.[47] The robot has four footpads made of poly(tetrafluoroethylene) (PTFE) film and glass fiber-reinforced plastic (GFRP). Its maximum leap height = 545 mm and takeoff velocity = 3.6 m/s, which are reported as the highest jumping performance on the water surface so far.

Figure 7. Rowing/walking and drag-dominant semiaquatic robots. (a) Schematic illustration of drag-dominant robots. (b) Scanning electron microscopy image of superhydrophobic nickel foam. (c) Hollow the footpad to increase buoyancy. (d) A water strider robot with superhydrophobic nickel foam sheets and a spring-based mechanism. L ≈ 0.15 m. (e) A water strider robot with a hollow ellipsoid structure for supporting and rotating mechanisms by a single motor. L ≈ 0.394 m. (f) An untethered water strider robot powered by servo motors. L ≈ 0.17 m. (b, d, e, f) Reprinted with permission from Reference 45. © 2012 ACS Publications, Reference 41. © 2012 IEEE, Reference 43. © 2022 IEEE, and Reference 44. © 2016 IEEE.

Figure 8. Surface tension-dominant and drag-dominant jumping robots. (a) A water strider robot with a torque-reversal mechanism. L ≈ 0.02 m. Reprinted with permission from Reference 5. © 2015 AAAS. (b) Roboleaper. L ≈ 0.013 m. Reprinted with permission from Reference 4. © 2007 Springer Nature. (c) A water strider robot with a latch driven by a shape-memory alloy actuator. L ≈ 0.15 m. Reprinted with permission from Reference 46. © 2008 IEEE. (d) A water strider robot capable of continuous jumping. L ≈ 0.26 m. Reprinted with permission from Reference 7. © 2016 IOP Publishing. (e) A water strider robot with drag pads. L ≈ 0.28 m. Reprinted with permission from Reference 47. © 2023 Springer Nature.

## Control of semiaquatic robots

Semiaquatic jumping robots and rowing/walking robots present distinctive opportunities and challenges regarding control issues. As previously discussed, jumping robots are capable of only a single jump, except for a particular jumping robot (Figure 8d) capable of performing multiple times. One of the difficulties for the multiple jumps lies in stable landing. The water strider robot (~26 cm) capable of multiple jumps has a footpad curved at the tip for stable landing. However, jumping on a smaller scale can be more difficult because the jumping organisms and robots are more vulnerable to rotating in the air than comparatively large counterparts given the same jumping height. As an example, a jumping robot (86 mg) rotates around 16 times in midair after jumping.[30] A springtail offers a possible solution to control in the air for stable jumping. The springtail forms a U-shape pose reducing body rotation for aerial righting. The springtail-inspired robot (terrestrial jumping robot) with drag flaps only rotates less than two times in midair showing the possibility of multiple jumps in an insect scale. Multiple jumping and stable landing on the water surface remains a challenge.

To date, rowing/walking robots have employed open-loop control based on various hydrodynamic and static models predicting the speed and travel distance of the robots. Control of these robots is performed only on still water except for a particular robot operated in the disturbance environment.[43] This robot demonstrated a large driving force to move in the disturbance environment with a wind speed of 2.3 m/s and a wave height of 210 mm. In the real aquatic environment, disturbances such as wind, waves, and obstacles are commonplace, which can disrupt the motion of the robots. To address these challenges, closed-loop control with sensors detecting the external environment can enhance a robot's performance in turbulent conditions.

Robot versus organism

We have explored various types of semiaquatic robots so far. We now move on to a quantitative evaluation of the speed of locomotion across different sizes. As previously mentioned, body scale is a critical factor that determines the mechanisms of reaction from the water surface involved in locomotion. For small organisms and robots, the utilization of surface tension force is sufficient for their movements on the water. However, this is not the case for larger bodies. Such bodies are required to generate more rapid movements to facilitate their motion, culminating in inertia-dominant drag. This pattern is demonstrated in **Figure 9**a–b, which represent organisms and robots, respectively. These plots provide a quantitative representation of body velocities, U, with body lengths, L. To the best of our knowledge, as referenced in Figure 9a–b, we lack small robots that exhibit body lengths comparable to that of small organisms
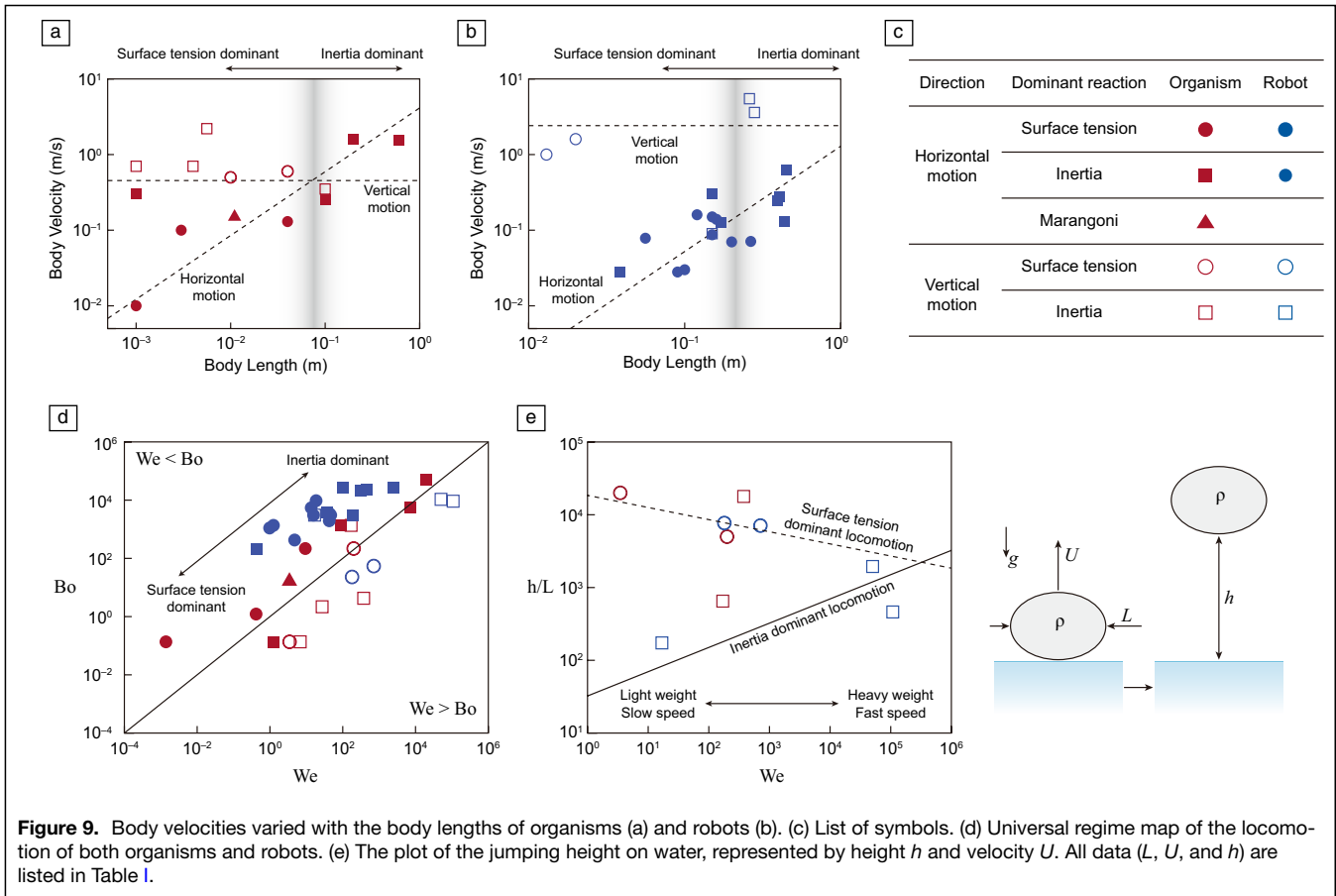
Figure 9. Body velocities varied with the body lengths of organisms (a) and robots (b). (c) List of symbols. (d) Universal regime map of the locomotion of both organisms and robots. (e) The plot of the jumping height on water, represented by height h and velocity U. All data (L, U, and h) are listed in Table I.

Table I. Data for Organisms and Robots.

		L (m)	U (m/s)	h (mm)	Reference
Organism	Springtail (*Anurida*)	0.001	0.01	N/A	9
	Water treader (*Mesovelia*)	0.003	0.1	N/A	48
	Water strider	0.04	0.13	N/A	3
	Microvelia	0.011	0.15	N/A	17
	Fisher spider	0.1	0.25	N/A	20
	Springtail (*I. retardatus*)	0.001	0.3	N/A	30
	Mallard duckling	0.6	1.53	N/A	28
	Basilisk lizard	0.2	1.6	N/A	25
	Water strider	0.028	1.5	200	47
	Springtail (*Podura aquatica*)	0.001	0.5	20	4
	Pygmy mole cricket	0.0056	2.2	100	49
	Fisher spider	0.1	0.9	65	50
	Fly	0.004	0.7	N/A	51
Robot	Yan et al.	0.12	0.16	N/A	37
	Zhang et al.	0.15	0.15	N/A	36
	Ozcan et al.	0.27	0.07	N/A	6
	Suzuki et al.	0.2	0.07	N/A	39
	Song et al.	0.1	0.03	N/A	35
	Yan et al.	0.16	0.14	N/A	38
	Song et al.	0.15	0.087	N/A	40
	Kim et al.	0.09	0.028	N/A	32
	Lee et al.	0.056	0.0783	N/A	34
	Chen et al.	0.0386	0.028	N/A	52
	Zhao et al.	0.15	0.3	N/A	41
	Huang et al.	0.438	0.129	N/A	53
	Yan et al.	0.394	0.243	N/A	42
	Zhang et al.	0.446	0.625	N/A	43
	Shihao et al.	0.17	0.1255	N/A	44
	Kim et al.	0.408	0.28	N/A	54
	Koh et al.	0.02	1.6	142	5
	Hu et al.	0.013	1	100	4
	Shin et al.	0.15	0.09	26	46
	Gwon et al.	0.28	3.6	545	47
	Yang et al.	0.26	5.476	120	7

U represents body velocity, *L* indicates body length, and *h* denotes jumping height.

due to a lack of fabrication technique. Figure 9c shows a list of various symbol meanings. We observe that the body velocity in the vertical direction remains largely consistent irrespective of body scales. However, when the object is moving in a horizontal direction, body velocity increases with increasing body length. We suspect that large robots and organisms need to perform more rapid strokes to jump their substantial bodies. Although it could appear that such rapid strokes would increase the body velocity, the presence of larger bodies with increased weight and drag could conversely result in a decrease in their body velocity. This suggests a tradeoff in the movement dynamics of large organisms and robots.

Using *U* (body velocity) and *L* (body length) as the characteristic velocity and length, respectively, results in the expressions for We = $\rho_l U^2 L/\gamma$ and Bo = $\rho_l L^2 g/\gamma$. Figure 9a–b shows a scatter plot of the data, but upon inspection, it becomes evident that all data points adhere to the trend line that represents the relationship Bo ~ We, as shown in Figure 9d. One can observe that the open symbols of the plot (vertical motion) are situated in the regime where We > Bo, where the inertia force surpasses the force of buoyancy. This fact could appear evident, yet it offers a profound understanding of vertical movements. Organisms and robots with larger mass could necessitate a stronger dynamic force related to *U* for executing a jumping on water, not merely relying on buoyancy.

As shown in Figure 9e, depending on the dominant hydrodynamic force of motion, the normalized maximum jumping height of natural and robotic systems, *h/L*, exhibits distinct relationships regarding morphological and dynamical scale (We). When the jumping motion at the interface is governed by surface tension force, jumping performance tends to decrease with increasing Weber number. Because the maximum force that the system can apply on the interface is limited so it should not break the water surface during the motion, the increased body length is inevitably associated with decreased normalized jumping height in these small systems. In contrast, as there is no upper limit in the drag force when the jumping motion is governed by the inertial force, an increase in Weber number results in enhanced jumping performance.

Conclusion and discussion

In summary, we have explored the design of semiaquatic robots that drew inspiration from the interfacial locomotion of organisms. Our initial focus centered on the physics of floating. Due to the capillary pressure between hairs, objects with a hairy morphology exhibit a significant advantage in maintaining stable flotation. Subsequently, we summarized the underlying mechanisms of interfacial locomotion. By examining the interplay of three key forces (F_i, F_s, and F_b), we were able to identify two dimensionless numbers (We and Bo) that serve as indicators for the dominant force behind the motions. However, it should be noted that due to the lack of reported data, when calculating dimensionless numbers, we used body speed rather than leg speed. This resulted in larger dimensionless numbers compared to the previous study.[9] Based on the mechanical study of locomotion, we conducted a review of a range of bioinspired robots, categorized by locomotion modes (horizontal and vertical). The robots also employ different dominant reaction forces to float on the water and move on the water surface depending on its scale. Analysis and optimization of the robot yield delicate and agile bioinspired robots that have potential applications in aquatic environmental investigation and rescue work. Furthermore, the robots designed in a small scale by a microfabrication process and high-power density material can prove how the semiaquatic organism interacts with and capitalizes on the water. This article shows different mechanisms arthropods move on water depending on the scale, and the engineered artifacts utilize these biohydrodynamics by the bioinspired design for achieving optimal

performance on water. In conclusion, we offered a universal plot incorporating both organisms and robots, based on dimensional analysis. For future research, the performance and efficiency of the system that interacts on the solid–fluid interface can be improved by the morphological design and dynamic control of systems based on the hydrodynamic scale as described in this article. The application expands to mobile robots, additive manufacturing systems, and coating processes in the industrial field that need to understand multiphase interaction.

Competing interests
The authors declare that they have no competing interests.

References
1. A.R. Parker, C.R. Lawrence, *Nature* **414**, 33 (2001)
2. A. Lee, M.-W. Moon, H. Lim, W.-D. Kim, H.-Y. Kim, *Langmuir* **28**, 10183 (2012)
3. D.L. Hu, B. Chan, J.W.M. Bush, *Nature* **424**, 663 (2003)
4. D.L. Hu, M. Prakash, B. Chan, J.W.M. Bush, *Exp. Fluids* **43**, 769 (2007)
5. J.-S. Koh, E. Yang, G.-P. Jung, S.-P. Jung, J.H. Son, S.-I. Lee, P.G. Jablonski, R.J. Wood, H.-Y. Kim, K.-J. Cho, *Science* **349**, 517 (2015)
6. O. Ozcan, H. Wang, J.D. Taylor, M. Sitti, *Int. J. Adv. Robot. Syst.* **11**, 85 (2014)
7. K. Yang, G. Liu, J. Yan, T. Wang, X. Zhang, J. Zhao, *Bioinspir. Biomim.* **11**, 066002 (2016)
8. J.W.M. Bush, D.L. Hu, M. Prakash, "The Integument of Water-walking Arthropods: Form and Function," in *Advances in Insect Physiology: Insect Mechanics and Control*, 1st ed., ed. by J. Casas, S.J. Simpson, Advances in Insect Physiology Series, vol. 34, ed. by S.J. Simpson (Academic Press, 2007), pp. 117–192
9. J.W.M. Bush, D.L. Hu, *Annu. Rev. Fluid Mech.* **38**, 339 (2005)
10. D. Vella, *Annu. Rev. Fluid Mech.* **47**, 115 (2015)
11. D. Vella, D.-G. Lee, H.-Y. Kim, *Langmuir* **22**, 5979 (2006)
12. D. Vella, P.D. Metcalfe, R.J. Whittaker, *J. Fluid Mech.* **549**, 215 (2006)
13. X. Gao, L. Jiang, *Nature* **432**, 36 (2004)
14. H.-M.S. Hu, G.S. Watson, B.W. Cribb, J.A. Watson, *J. Exp. Biol.* **214**, 915 (2011)
15. H.Y. Erbil, C.E. Cansoy, *Langmuir* **25**, 14135 (2009)
16. T.-G. Cha, J.W. Yi, M.-W. Moon, K.-R. Lee, H.-Y. Kim, *Langmuir* **26**, 8319 (2010)
17. L.J. Burton, N. Cheng, J.W. Bush, *Integr. Comp. Biol.* **54**, 969 (2014)
18. C. Lang, K. Seifert, K. Dettner, *Naturwissenschaften* **99**, 937 (2012)
19. D.L. Hu, J.W.M. Bush, *J. Fluid Mech.* **644**, 5 (2010)
20. R.B. Suter, *J. Arachnol.* **27**, 489 (1999)
21. Z. Hu, W. Fang, Q. Li, X.-Q. Feng, J.-A. Lv, *Nat. Commun.* **11**, 5780 (2020)
22. E. Yang, J.H. Son, S.-I. Lee, P.G. Jablonski, H.-Y. Kim, *Nat. Commun.* **7**, 13698 (2016)
23. H.-Y. Kim, J. Amauger, H.-B. Jeong, D.-G. Lee, E. Yang, P.G. Jablonski, *Phys. Rev. Fluids* **2**, 100505 (2017)
24. R.B. Suter, *J. Arachnol.* **41**, 93 (2013)
25. J.W. Glasheen, T.A. McMahon, *Nature* **380**, 340 (1996)
26. J.W. Glasheen, T.A. McMahon, *J. Exp. Biol.* **199**, 2611 (1996)
27. S.T. Hsieh, G.V. Lauder, *J. Exp. Biol.* **101**, 16784 (2004)
28. T. Aigeldinger, F. Fish, *J. Exp. Biol.* **198**, 1567 (1995)
29. W.T. Gough, S.C. Farina, F.E. Fish, *J. Exp. Biol.* **218**, 1632 (2015)
30. V.M. Ortega-Jimenez, E.J. Challita, B. Kim, H. Ko, M. Gwon, J.-S. Koh, M.S. Bhamla, *Proc. Natl. Acad. Sci. U.S.A.* **119**, e2211283119 (2022)
31. W. Kim, J. Amauger, J. Ha, T.H. Pham, A.D. Tran, J.H. Lee, J. Park, P.G. Jablonski, H.-Y. Kim, S.-I. Lee, *Proc. Natl. Acad. Sci. U.S.A.* **120**, e2219972120 (2023)
32. D. Kim, M. Gwon, B. Kim, V.M. Ortega-Jimenez, S. Han, D. Kang, M.S. Bhamla, J.-S. Koh, *Micromachines* (Basel) **13**(4), 627 (2022)
33. D. Kim, B. Kim, B. Shin, D. Shin, C.-K. Lee, J.-S. Chung, J. Seo, Y.-T. Kim, G. Sung, W. Seo, S. Kim, S. Hong, S. Hwang, S. Han, D. Kang, H.-S. Lee, J.-S. Koh, *Nat. Commun.* **13**, 4155 (2022)
34. K.Y. Lee, L. Wang, J. Qu, K.R. Oldham, "Milli-scale Biped Vibratory Water Strider," *2019 International Conference on Manipulation, Automation and Robotics at Small Scales (MARSS)* (IEEE, Helsinki, July 1–5, 2019), pp. 1–6
35. Y.S. Song, M. Sitti, *IEEE Trans. Robot.* **23**, 578 (2007)
36. X. Zhang, J. Zhao, Q. Zhu, N. Chen, M. Zhang, Q. Pan, *ACS Appl. Mater. Interfaces* **3**, 2630 (2011)
37. J.H. Yan, X.B. Zhang, J. Zhao, G.F. Liu, H.G. Cai, Q.M. Pan, *Bioinspir. Biomim.* **10**, 046016 (2015)
38. J. Yan, K. Yang, G. Liu, J. Zhao, *IEEE Access* **8**, 89643 (2020)
39. K. Suzuki, H. Takanobu, K. Noya, H. Koike, H. Miura, "Water Strider Robots with Microfabricated Hydrophobic Legs," *2007 IEEE/RSJ International Conference on Intelligent Robots and Systems* (San Diego, October 29–November 2, 2007), pp. 590–595
40. Y.S. Song, M. Sitti, "STRIDE; A Highly Maneuverable and Non-tethered Water Strider Robot," in *Proceedings of the 2007 IEEE International Conference on Robotics and Automation* (Rome, 2007), pp. 980–984
41. J. Zhao, X. Zhang, Q. Pan, "A Water Walking Robot Inspired by Water Strider," *2012 IEEE International Conference on Mechatronics and Automation* (Chengdu, August 5–8, 2012), pp. 962–967
42. J. Yan, X. Zhang, K. Yang, J. Zhao, "A Single Driven Bionic Water Strider Sliding Robot Mimicking the Spatial Elliptical Trajectory," *2019 IEEE International Conference on Robotics and Biomimetics (ROBIO)* (Dali, Yunnan, December 6–8, 2019), pp. 142–147
43. X. Zhang, J. Yan, K. Yang, J. Zhao, S. Tang, *IEEE Robot. Autom. Lett.* **7**, 2463 (2022)
44. Z. Shihao, J. Chen, D. Li, W. Ge, J. Leng, H. Huang, "Mechanical Design and Experimental Research on Locomotion Characters of Robot Inspired by Water Strider," *2016 6th IEEE International Conference on Biomedical Robotics and Biomechatronics (BioRob)* (Singapore, June 26–29, 2016), pp. 145–150
45. J. Zhao, X. Zhang, N. Chen, Q. Pan, *ACS Appl. Mater. Interfaces* **4**, 3706 (2012)
46. B. Shin, H-Y. Kim, K.-J. Cho, "Towards a Biologically Inspired Small-Scale Water Jumping Robot," *2008 2nd IEEE RAS & EMBS International Conference on Biomedical Robotics and Biomechatronics (BioRob)* (Scottsdale, October 19–22, 2008), pp. 127–131
47. M. Gwon, D. Kim, B. Kim, S. Han, D. Kang, J.-S. Koh, *Nat. Commun.* **14**, 1473 (2023)
48. A.J.J. Crumière, M.E. Santos, M. Sémon, D. Armisén, F.F.F. Moreira, A. Khila, *Curr. Biol.* **26**, 3336 (2016)
49. M. Burrows, G.P. Sutton, *Curr. Biol.* **22**, R990 (2012)
50. B.S. Robert, G. Jessica, *J. Arachnol.* **28**, 201 (2000)
51. M. Burrows, *J. Exp. Biol.* **216**, 1973 (2013)
52. Y. Chen, N. Doshi, B. Goldberg, H. Wang, R.J. Wood, *Nat. Commun.* **9**, 2495 (2018)
53. H. Huang, C. Sheng, G. Wu, Y. Shen, H. Wang, *Appl. Sci.* (Basel) **10**(18), 6300 (2020)
54. H. Kim, D. Lee, K. Jeong, T. Seo, *IEEE/ASME Trans. Mechatron.* **21**, 175 (2016) ☐

Dongjin Kim is a doctoral candidate in the Department of Mechanical Engineering at Ajou University, South Korea. He received his BS degree from the Department of Mechanical Engineering at Ajou University in 2018. His research focuses on artificial muscle actuators for application in microrobotics, soft robotics, and wearable devices. Kim can be reached by email at rlaehdwlswt@ajou.ac.kr.
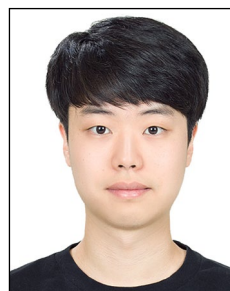
Chan Jin Park is a postdoctoral research associate in the Department of Chemical and Biological Engineering at Princeton University. He received his BS and PhD degrees from Seoul National University, South Korea, in naval architecture and ocean engineering and mechanical engineering. His research interests include microfluid mechanics, biomimetics, and soft-matter physics. Park can be reached by email at cp4553@princeton.edu.

Je-Sung Koh is currently an associate professor of mechanical engineering at Ajou University, South Korea. He received his BS and PhD degrees in mechanical and aerospace engineering from Seoul National University, South Korea, in 2008 and 2014, respectively. He was a post-doctoral fellow with Harvard Microrobotics Laboratory until 2017. His research interests include biologically inspired, small-scale robot design and soft robotics. Koh can be reached by email at jskoh@ajou.ac.kr.

Jonghyun Ha is an assistant professor at Ajou University, South Korea. He received his BS degree from Chungnam National University, South Korea, in 2012, and PhD degree from Seoul National University, South Korea, in 2018. He completed postdoctoral research at the University of Illinois at Urbana-Champaign in 2021, then joined the Samsung Advanced Institute of Technology. By 2022, he transitioned to his current role at Ajou University. His research interests include microfluids, porous flows, and micro-scale fluid–solid interactions. Ha can be reached by email at hajh@ajou.ac.kr.